ADVANCED MATERIALS

www.advmat.de

In Situ Back-Contact Passivation Improves Photovoltage and Fill Factor in Perovskite Solar Cells

Furui Tan, Hairen Tan, Makhsud I. Saidaminov, Mingyang Wei, Mengxia Liu, Anyi Mei, Peicheng Li, Bowen Zhang, Chih-Shan Tan, Xiwen Gong, Yongbiao Zhao, Ahmad R. Kirmani, Ziru Huang, James Z. Fan, Rafael Quintero-Bermudez, Junghwan Kim, Yicheng Zhao, Oleksandr Voznyy, Yueyue Gao, Feng Zhang, Lee J. Richter, Zheng-Hong Lu, Weifeng Zhang,* and Edward H. Sargent**

Organic–inorganic hybrid perovskite solar cells (PSCs) have seen a rapid rise in power conversion efficiencies in recent years; however, they still suffer from interfacial recombination and charge extraction losses at interfaces between the perovskite absorber and the charge–transport layers. Here, in situ back-contact passivation (BCP) that reduces interfacial and extraction losses between the perovskite absorber and the hole transport layer (HTL) is reported. A thin layer of nondoped semiconducting polymer at the perovskite/HTL interface is introduced and it is shown that the use of the semiconductor polymer permits—in contrast with previously studied insulator-based passivants—the use of a relatively thick passivating layer. It is shown that a flat-band alignment between the perovskite and polymer passivation layers achieves a high photovoltage and fill factor: the resultant BCP enables a photovoltage of 1.15 V and a fill factor of 83% in 1.53 eV bandgap PSCs, leading to an efficiency of 21.6% in planar solar cells.

As a promising low-cost photovoltaic technology, organic–inorganic perovskite solar cells (PSCs) have recently reached a certified power conversion efficiency (PCE) of 23.7%.[1] The rapid increase in PCE has been achieved as a result of extensive research on perovskite composition engineering,[2–5] film crystallization process,[6–9] and carrier-selective charge transport layers.[10–14]

The performance of solar cells relies on efficient charge carrier extraction at interfaces.[15–19] The electron transport layer (ETL) and hole transport layer (HTL) are typically heavily doped to ensure sufficient conductivity; however, this high doping also leads to higher recombination losses at perovskite/ETL(HTL) interfaces.[20–22]

Interface engineering in PSCs has been studied in the context of n-i-p structured cells,[20–25] specifically in situ passivation and posttreatment of the ETL prior to the deposition of perovskite.[10,26–32] The bottom n-type ETL is usually a robust material (e.g., TiO_2 or SnO_2) that is highly tolerant to the surface treatment. For example, in previous work, Cl-capped TiO_2 nanocrystals were deployed to achieve front contact passivation at the ETL/perovskite interface.[10]

Contact passivation atop the as-deposited perovskite absorber layer (**Figure 1**a), i.e., at the perovskite/HTL interface in n-i-p devices, requires more delicate chemical treatment in light of the chemical vulnerability of perovskites. Implementing contact passivation at the perovskite/HTL interface in n-i-p structured solar cells seeks to suppress this interfacial recombination loss while still enabling efficient hole extraction.

Dr. F. Tan, Prof. H. Tan, Dr. M. I. Saidaminov, M. Wei, Dr. M. Liu, Dr. A. Mei, Dr. C.-S. Tan, Dr. X. Gong, Dr. Y. Zhao, Z. Huang, J. Z. Fan, R. Quintero-Bermudez, Dr. J. Kim, Dr. Y. Zhao, Prof. O. Voznyy, Prof. E. H. Sargent
Department of Electrical and Computer Engineering
University of Toronto
Toronto, Ontario M5S 3G4, Canada
E-mail: hairentan@nju.edu.cn; ted.sargent@utoronto.ca

Dr. F. Tan, Dr. B. Zhang, Dr. Y. Gao, Dr. F. Zhang, Prof. W. Zhang
Key Laboratory of Photovoltaic Materials
Department of Physics and Electronics
Henan University
Kaifeng, Henan 475004, China
E-mail: wfzhang@henu.edu.cn

The ORCID identification number(s) for the author(s) of this article can be found under https://doi.org/10.1002/adma.201807435.

Prof. H. Tan
National Laboratory of Solid State Microstructures
Jiangsu Key Laboratory of Artificial Functional Materials
College of Engineering and Applied Sciences
Nanjing University
Nanjing 210093, China

P. Li, Dr. Y. Zhao, Prof. Z.-H. Lu
Department of Materials Science and Engineering
University of Toronto
184 College Street, Toronto, Ontario M5S 3E4, Canada

Dr. A. R. Kirmani, Prof. L. J. Richter
Materials Science and Engineering Division
National Institute of Standards and Technology (NIST)
Gaithersburg, MD 20899, USA

DOI: 10.1002/adma.201807435

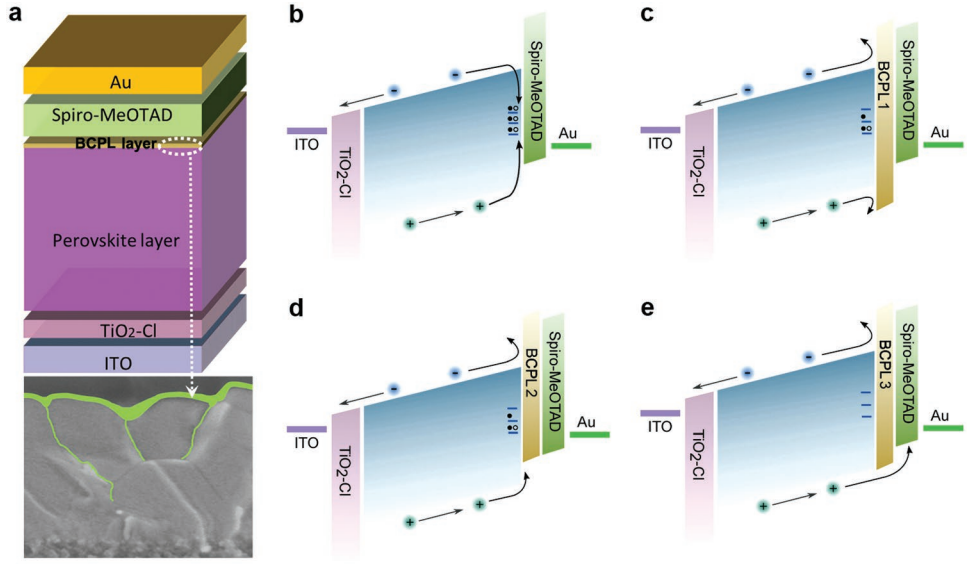

Figure 1. Device structure of PSCs with BCP. a) Schematic device structure of PSC with a BCPL. b–e) PSCs without and with BCPL with three possible energy level alignments between the perovskite and BCPL.

An insulating layer at the perovskite/HTL interface has been shown to increase the open-circuit voltage (V_{oc}) in PSCs,[25,33–35] but at a cost to fill factor. When an insulator is used, the passivation layer needs to be sufficiently thin—circa 1 nm—to allow hole tunneling. Since solution-processed perovskite surfaces have a roughness of tens of nanometers, this makes the insulator thickness difficult to control.

These considerations motivate a back-contact passivation (BCP) strategy that does not compromise fill factor.[16] Given the success of passivating contacts that use intrinsic amorphous silicon in record-efficiency crystalline silicon photovoltaics,[36,37] here we pursued an in situ BCP approach based on an intrinsic (undoped) thin semiconducting polymer. We report that the semiconducting nature of polymers, along with their band alignment with perovskites, plays a key role in achieving the combination of high photovoltage and fill factor. By applying this BCP design, we achieve a V_{oc} of 1.15 V, a fill factor of 83%, and a stabilized PCE of 21.6% in 1.53 eV bandgap planar PSCs—among the highest efficiencies reported in planar devices.

In an n-i-p PSC, nonradiative recombination at the perovskite/HTL interface is a source of loss due to high defect densities at the perovskite surface at its interface with the heavily doped HTL (i.e., Li-salt doped Spiro-OMeTAD). The BCP layer (BCPL) strives for optimized recombination and extraction dynamics at this interface (Figure 1a). The thin semiconducting polymer layer suppresses recombination through chemical or physical passivation, and relies on a judicious choice of highest occupied molecular orbital (HOMO) levels within different polymers (Figure 1b–e).

We considered three scenarios for BCPLs. In a first scenario (Figure 1c), the insulating polymer may provide passivation, but provides no charge-selection function and only allows carrier tunneling for transport. In a second scenario (Figure 1d), the semiconducting polymer has a HOMO level shallower than that of the perovskite, providing a large driving force for hole extraction. In a third scenario (Figure 1e), the HOMO of the semiconducting polymer is aligned with that of the perovskite film, and this enables energy-lossless hole extraction at the interface.

With these energy level alignment scenarios in mind, we chose three polymers as candidate BCPLs, each of which corresponds to one scenario (**Figure 2**a): poly(vinylidene fluoride-co-hexafluoropropylene) (PVDF-HFP) with a deep HOMO of −7.2 eV; poly[bis(4-phenyl)(2,4,6-trimethylphenyl) amine] (PTAA) with a shallow HOMO of −5.1 eV, shallower than the perovskite; and poly(4-butylphenyldiphenylamine) (PTPD) with a HOMO of −5.5 eV, well-aligned with that of the perovskite (Figures S1, S2, and Table S1, Supporting Information).

We fabricated polymer-passivated perovskite films by in situ depositing the polymers in the antisolvent. We first checked for the presence of polymers (e.g., PTPD) on perovskite films. Scanning electron microscopy (SEM) images and Fourier-transform infrared spectroscopy (FTIR) spectra show that the PTPD is indeed present (Figure 2b and Figure S3, Supporting Information). Furthermore, when we used fluorine as an elemental marker in PVDF-HFP and performed time-of-flight secondary ion mass spectrometry (TOF-SIMS; Figure S4, Supporting Information) and energy-dispersive X-ray mapping (Figure S5, Supporting Information), we found a uniform distribution of polymer on perovskite surface.

We then investigated whether the polymer is washed away using chlorobenzene, a solvent used in the processing of Spiro-OMeTAD during the fabrication of solar cells. As-prepared and chlorobenzene-treated perovskite films showed no observable differences in SEM (Figure S3, Supporting Information) and ultraviolet photoelectron spectroscopy measurements (Figure S6, Supporting Information), we conclude that the perovskite remains covered with a layer of polymer following the deposition of Spiro-OMeTAD.

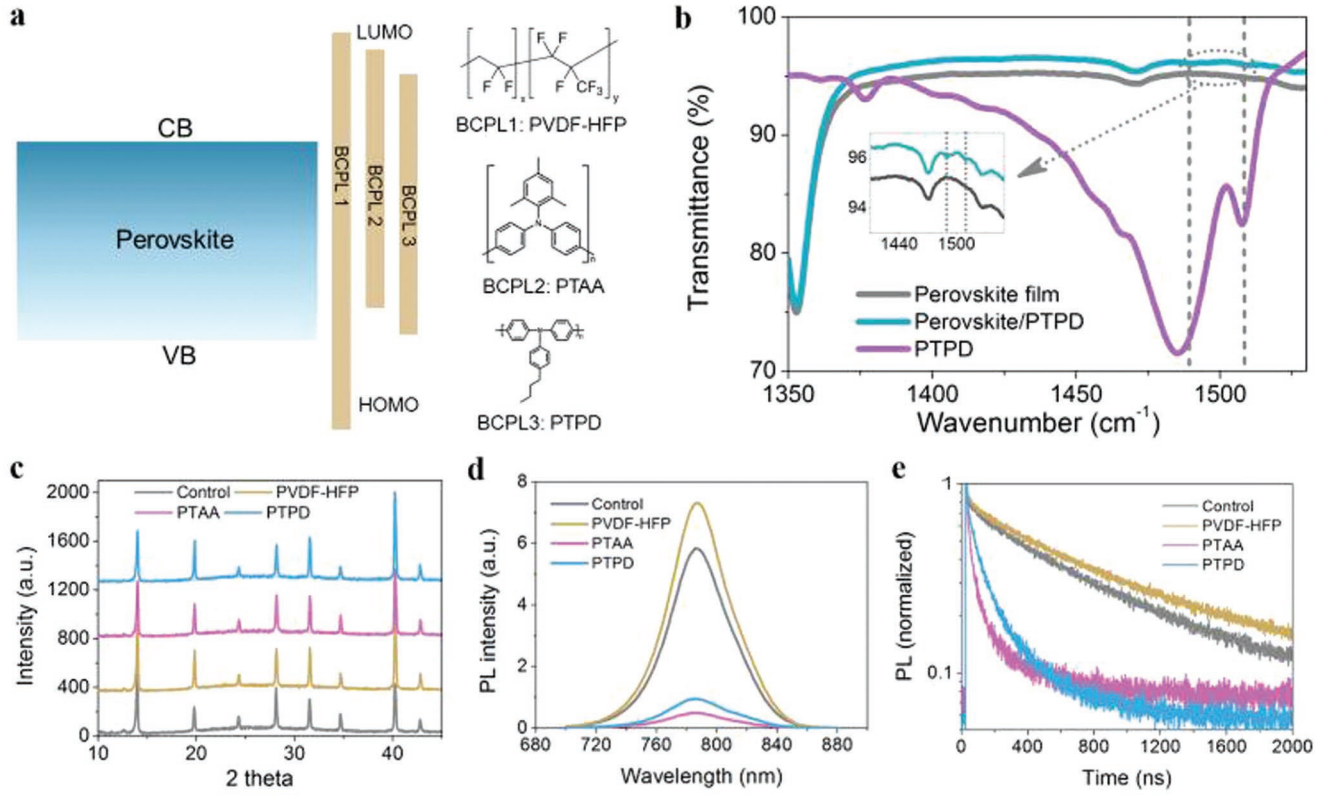

Figure 2. The BCPL materials and their influence on charge extraction dynamics. a) The three polymers and their energy level alignments with perovskite. b) FTIR spectra of perovskite films with and without the BCPL. c) XRD of perovskite films without and with BCPLs. d) Steady-state photoluminescence (PL) and e) time-resolved PL spectra of perovskite films on glass substrate.

We then investigated the influence of BCPLs on the crystal structure and morphology of perovskites. X-ray powder diffraction (XRD) measurements confirm similar crystallinity for perovskite films without and with BCPLs (Figure 2c). Grazing incidence wide-angle X-ray scattering also showed no significant changes both in in-plane crystallographic structure and texture of the perovskite samples (Figure S7, Supporting Information). SEM images show similar surface morphology of the different samples with densely packed grains and pinhole-free films (Figure S8, Supporting Information).

To study charge transfer dynamics, we carried out steady-state and time-resolved photoluminescence (PL) measurements (Figure 2d). PVDF-HFP substantially increases PL intensity compared to control films, while PTAA and PTPD reduce PL. The enhanced PL intensity suggests that PVDF-HFP does not induce charge transfer—likely a consequence of its insulating nature—but that it does passivate defects on the perovskite surface. This we attribute to chemical coordination between the strongly polar fluorine terminal groups and the under-coordinated Pb^{2+} ions. This agrees with the prolonged PL lifetime of PVDF-HFP samples compared to control films (Figure 2e and Table S2, Supporting Information). Given the type-II energy level alignment of PTAA and PTPD with perovskite, the observed PL quenching with these polymers is unlikely to be due to increased nonradiative recombination;[22] instead, we propose that is more likely due to efficient charge transfer.[23,38–40] The PL quenches further when we added an extra HTL, doped Spiro-OMeTAD, atop perovskite films (Figure S9, Supporting Information). Time-resolved PL results follow the same trend: PTAA and PTPD shorten the PL lifetime, and a further accelerated decay takes place for samples with a Spiro-OMeTAD-based HTL on top (Figure 2e, Figure S9, and Table S2, Supporting Information). In sum, the insulating polymer PVDF-HFP prevents hole extraction; whereas PTAA and PTPD do allow for hole extraction. PTAA quenches PL more than PTPD does, as the former has a 0.3 eV shallower HOMO level than the latter.

We then fabricated PSCs using the various BCPLs. The statistical performance for each case from 60 devices is summarized in **Figure 3**a and **Table 1**. Solar cells with PTPD exhibit the highest average PCE among the four kinds of devices, with the improvement coming from V_{oc} and FF. The control devices (without BCPL) have an average V_{oc} of 1.113 V, a J_{sc} of 22.4 mA cm^{-2}, an FF of 78.7%, and a PCE of 19.6%. The devices with PTAA present a similar average PCE of 20.0% while the adoption of PVDF decreases the averaged PCE to 19.1%. Devices with PTPD achieve the highest average PCE of 20.9%, with an improved average V_{oc} of 1.129 V and FF of 80.7%.

We note that the performance of cells with PVDF-HFP is more sensitive to the polymer concentration than that of devices with other semiconducting polymers (Figure S10, Supporting Information). We attribute this to the insulating nature of PVDF-HFP. Although V_{oc} is expected to increase with PVDF-HFP due to the interfacial passivation, the incorporation of

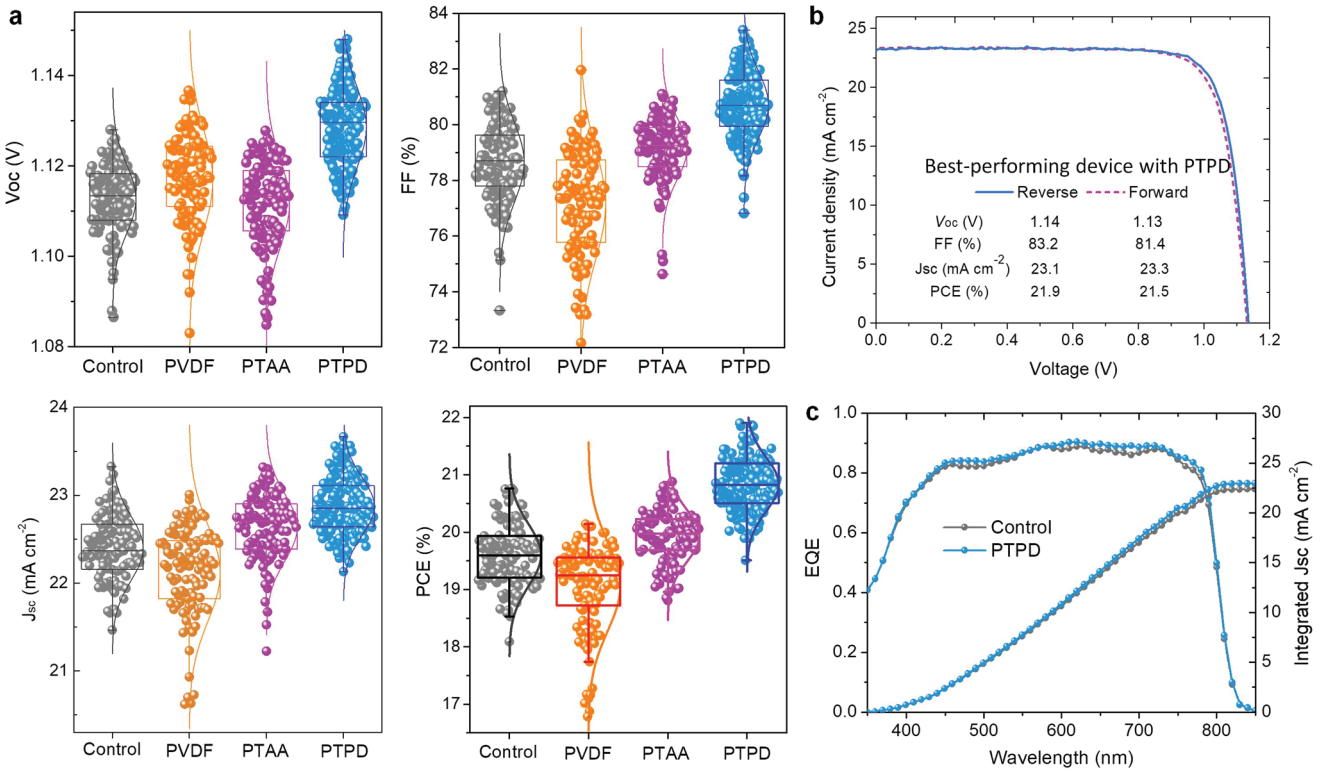

Figure 3. Statistics of solar cell performance with and without BCPLs. a) Photovoltaic parameters of solar cells. The whisker range is outlier and the whisker coef. is 1.5 for all the statistics. b) *J–V* curves of the best-performing solar cells with PTPD. c) EQE and integrated current density of the control device and the cell with PTPD.

a thin layer of insulating polymer reduces the FF because of higher resistance. In contrast, the adoption of semiconducting polymers (i.e., PTPD) allows thicker passivating films (and thus better surface coverage on rough perovskite films) to boost the photovoltaic performance.

The best-performing cells with PTPD showed a stabilized PCE of 21.6% (Figure 3b and Figure S11, Supporting Information). The integrated J_{sc} from external quantum efficiency (EQE) spectra is 23.0 mA cm^{-2} and 22.5 mA cm^{-2} for the devices with and without PTPD, respectively, matching well with the values from *J–V* measurements (Figure 3c and Table 1). The slight increase in J_{sc} for the PTPD cells is attributed to the combined benefits of suppression of interfacial recombination, and the facilitation of hole extraction via the cascade type-II HOMO level alignment at the perovskite/PTPD/hole transporting material interface in the solar cells.

Table 1. Photovoltaic performance of solar cells.

Device	V_{oc} [V]	J_{sc} [mA cm^{-2}]	FF [%]	PCE [%]
Control	1.11 ± 0.01[a)]	22.4 ± 0.4	78.7 ± 1.4	19.6 ± 0.5
Control best	1.128	22.7	81.6	20.9
PVDF	1.12 ± 0.01	22.2 ± 0.5	77.2 ± 2.0	19.1 ± 0.8
PVDF best	1.131	22.4	79.3	20.1
PTAA	1.11 ± 0.01	22.7 ± 0.4	79.2 ± 1.1	20.0 ± 0.5
PTAA best	1.126	23.2	79.8	20.9
PTPD	1.13 ± 0.01	22.9 ± 0.3	80.7 ± 1.2	20.9 ± 0.5
PTPD best	1.137	23.1	83.2	21.9

[a)]± represents standard deviation of the mean.

We sent a device with PTPD, without encapsulation, to an accredited independent photovoltaics test laboratory (Newport Corporation PV Lab, Montana, USA) and it produced a certified efficiency of 20.8% (Figure S12, Supporting Information); the lower performance and the hysteresis observed during certification may be due to the degradation of solar cells during sample shipping.

We also tested the operational stability at the maximum power point under UV-filtered AM1.5G illumination (100 mW cm^{-2}, with a 420 nm cutting-off UV filter). To emulate solar cell working conditions,[41] we tested the devices at 1 sun MPP for 10 h and then stored for 13 h under dark in the air (Figure S13, Supporting Information). The device with PTPD exhibits improved stability compared to the control device and retains 90% of its initial efficiency following 80 h MPP tracking (corresponding to 175 h stability test).

We next characterized solar cells by various electro-optical methods (**Figure 4**a). Transient photovoltage showed a decay lifetime of 6.9, 8.8, 14.5, and 16.7 µs for the control, PTAA-, PTPD-, and PVDF-HFP-passivated cells, respectively. Impedance spectra show, for all polymer-passivated devices, charge transfer recombination resistance (R_{tr}) values that are larger than those seen in the control devices (Figure 4b and Figure S14,

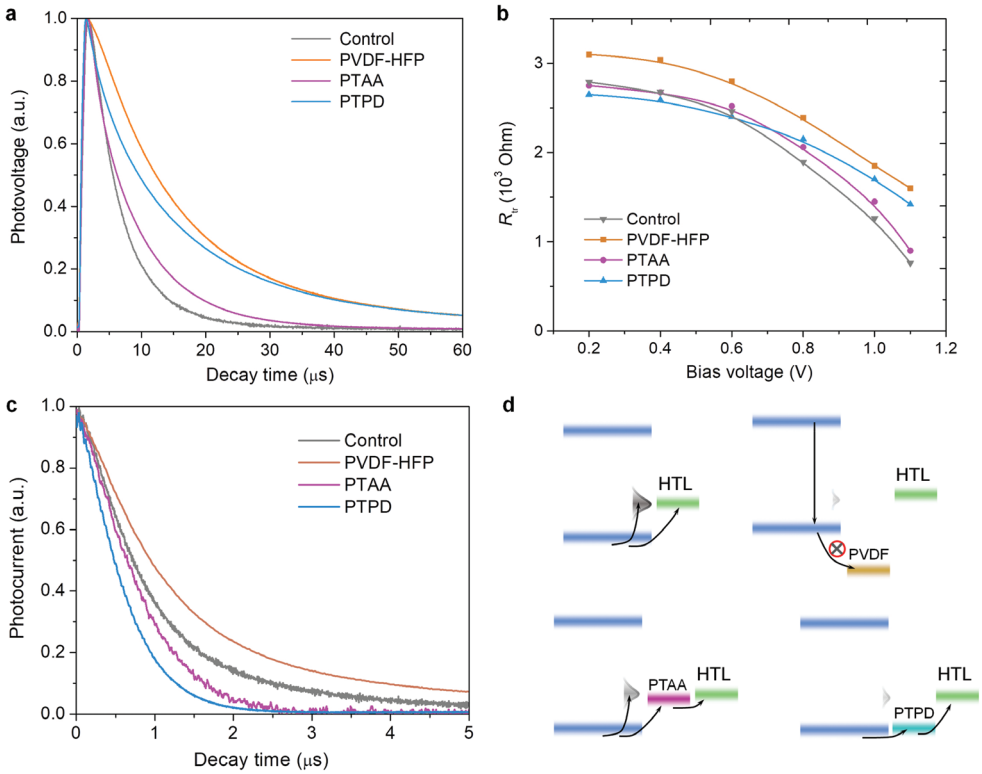

Figure 4. Charge dynamics in perovskite/passivant structures. a) Transient photovoltage decay of the control cell and the cells with different BCPLs. b) Electrochemistry impedance spectra, c) transient photocurrent decay, and d) energy level diagrams of the four cells.

Supporting Information). We measured photocurrent decay lifetime of 0.97, 0.84, 0.63, and 1.34 μs for the control, PTAA, PTPD, and PVDF-HFP cells, respectively. These results are consistent with the PL results seen in the perovskite films as discussed above.[42,43]

We show the process of hole extraction in Figure 4d. Although 310 mV HOMO offset at perovskite/PTAA interface in principle provides the largest driving force for charge transfer, it also leads to increased energy loss, which is detrimental for V_{oc}. PVDF-HFP, in turn, builds a large barrier (>2.0 eV) for hole extraction, which works against high FF. A favorable BCPL, such as PTPD, shall effectively passivate back contact and flatten energy extraction, resulting in optimal photovoltaic performance. We measured the ideality factor, an indication of Shockley–Read–Hall (trap-assisted) recombination: PTPD cells showed a factor of 1.4, while the control cells 1.8 (Figure S15, Supporting Information).

In conclusion, this work explores in situ BCP in n-i-p planar PSCs. Charge dynamics are modulated through introduction of an intrinsic thin semiconducting polymer layer at the perovskite/HTL interface. We find that the photovoltaic performance depends on the band alignment between perovskite and BCPLs. Solar cells with PTPD BCPL generates an enhanced stabilized PCE of 21.6% with a remarkable FF of 83%. Certified efficiency of 20.8% was achieved based on this in situ BCP strategy. The favorable photovoltaic improvement is attributed to effective suppression of charge recombination as well as facilitated hole extraction at the perovskite/HTL interface.

Supporting Information

Supporting Information is available from the Wiley Online Library or from the author.

Acknowledgements

F.T. and H.T. contributed equally to this work. This publication is based in part on work supported by the US Office of Naval Research (Grant Award No.: N00014-17-1-2524), by the Ontario Research Fund Research Excellence Program, and by the Natural Sciences and Engineering Research Council (NSERC) of Canada. The work of F.T. was also supported by the China Scholarship Council (201608410244). This work was also supported by the National Natural Science Foundation of China (Grant no. 61306019), the Natural Science Foundation of Henan Province (Grant no. 162300410026), the Key Member of Young Teachers (Grant no. 2016GGJS-019), and the Henan University Fund. H.T. acknowledges the Rubicon grant (680-50-1511) from the Netherlands Organisation for Scientific Research (NWO) and the National 1000 Young Talents award in China. The authors thank P. M. Brodersen from Ontario Centre for Characterization of Advanced Materials (OCCAM) for TOF-SIMS measurements and analysis. Beamline 7.3.3 of the Advanced Light Source was supported by the Director of the Office of Science, Office of Basic Energy Sciences, of the U.S. Department of Energy under Contract No. DE-AC02-05CH11231. M.I.S. acknowledges the support of the Banting Postdoctoral Fellowship Program, administered by the Government of Canada.

Conflict of Interest

The authors declare no conflict of interest.

Keywords

band alignment, passivation, perovskite solar cells, semiconducting polymers

Received: November 16, 2018
Revised: January 14, 2019
Published online:

[1] https://www.nrel.gov/pv/assets/pdfs/pv-efficiency-chart.20190103.pdf (accessed: January 2019).
[2] W. S. Yang, B.-W. Park, E. H. Jung, N. J. Jeon, Y. C. Kim, D. U. Lee, S. S. Shin, J. Seo, E. K. Kim, J. H. Noh, S. I. Seok, *Science* **2017**, *356*, 1376.
[3] M. Saliba, T. Matsui, K. Domanski, J.-Y. Seo, A. Ummadisingu, S. M. Zakeeruddin, J.-P. Correa-Baena, W. R. Tress, A. Abate, A. Hagfeldt, M. Grätzel, *Science* **2016**, *354*, 206.
[4] M. Abdi-Jalebi, Z. Andaji-Garmaroudi, S. Cacovich, C. Stavrakas, B. Philippe, J. M. Richter, M. Alsari, E. P. Booker, E. M. Hutter, A. J. Pearson, S. Lilliu, T. J. Savenije, H. Rensmo, G. Divitini, C. Ducati, R. H. Friend, S. D. Stranks, *Nature* **2018**, *555*, 497.
[5] M. I. Saidaminov, J. Kim, A. Jain, R. Quintero-Bermudez, H. Tan, G. Long, F. Tan, A. Johnston, Y. Zhao, O. Voznyy, E. H. Sargent, *Nat. Energy* **2018**, *3*, 648.
[6] X. Li, D. Bi, C. Yi, J.-D. Décoppet, J. Luo, S. M. Zakeeruddin, A. Hagfeldt, M. Grätzel, *Science* **2016**, *353*, 58.
[7] C. Bi, Q. Wang, Y. Shao, Y. Yuan, Z. Xiao, J. Huang, *Nat. Commun.* **2015**, *6*, 7747.
[8] D. Bi, C. Yi, J. Luo, J.-D. Décoppet, F. Zhang, S. M. Zakeeruddin, X. Li, A. Hagfeldt, M. Grätzel, *Nat. Energy* **2016**, *1*, 16142.
[9] W. Kim, M. S. Jung, S. Lee, Y. J. Choi, J. K. Kim, S. U. Chai, W. Kim, D.-G. Choi, H. Ahn, J. H. Cho, D. Choi, H. Shin, D. Kim, J. H. Park, *Adv. Energy Mater.* **2018**, *8*, 1702369.
[10] H. Tan, A. Jain, O. Voznyy, X. Lan, F. P. G. d. Arquer, J. Z. Fan, R. Quintero-Bermudez, M. Yuan, B. Zhang, Y. Zhao, F. Fan, P. Li, L. N. Quan, Y. Zhao, Z.-H. Lu, Z. Yang, S. Hoogland, E. H. Sargent, *Science* **2017**, *355*, 722.
[11] S. S. Shin, E. J. Yeom, W. S. Yang, S. Hur, M. G. Kim, J. Im, J. Seo, J. H. Noh, S. I. Seok, *Science* **2017**, *356*, 167.
[12] N. J. Jeon, H. Na, E. H. Jung, T.-Y. Yang, Y. G. Lee, G. Kim, H.-W. Shin, S. Il Seok, J. Lee, J. Seo, *Nat. Energy* **2018**, *3*, 682.
[13] J. A. Christians, P. Schulz, J. S. Tinkham, T. H. Schloemer, S. P. Harvey, B. J. Tremolet de Villers, A. Sellinger, J. J. Berry, J. M. Luther, *Nat. Energy* **2018**, *3*, 68.
[14] Q. Jiang, L. Zhang, H. Wang, X. Yang, J. Meng, H. Liu, Z. Yin, J. Wu, X. Zhang, J. You, *Nat. Energy* **2017**, *2*, 16177.
[15] G.-J. A. H. Wetzelaer, M. Scheepers, A. M. Sempere, C. Momblona, J. Ávila, H. J. Bolink, *Adv. Mater.* **2015**, *27*, 1837.
[16] J.-P. Correa-Baena, W. Tress, K. Domanski, E. H. Anaraki, S.-H. Turren-Cruz, B. Roose, P. P. Boix, M. Grätzel, M. Saliba, A. Abate, A. Hagfeldt, *Energy Environ. Sci.* **2017**, *10*, 1207.
[17] Y. Lin, B. Chen, F. Zhao, X. Zheng, Y. Deng, Y. Shao, Y. Fang, Y. Bai, C. Wang, J. Huang, *Adv. Mater.* **2017**, *29*, 1700607.
[18] S. Yue, K. Liu, R. Xu, M. Li, M. Azam, K. Ren, J. Liu, Y. Sun, Z. Wang, D. Cao, X. Yan, S. Qu, Y. Lei, Z. Wang, *Energy Environ. Sci.* **2017**, *10*, 2570.
[19] A. R. Kirmani, A. D. Sheikh, M. R. Niazi, M. A. Haque, M. Liu, F. P. G. de Arquer, J. Xu, B. Sun, O. Voznyy, N. Gasparini, D. Baran, T. Wu, E. H. Sargent, A. Amassian, *Adv. Mater.* **2018**, *30*, 1801661.
[20] Y. Yang, M. Yang, D. T. Moore, Y. Yan, E. M. Miller, K. Zhu, M. C. Beard, *Nat. Energy* **2017**, *2*, 16207.
[21] H. Zhou, Q. Chen, G. Li, S. Luo, T.-b. Song, H.-S. Duan, Z. Hong, J. You, Y. Liu, Y. Yang, *Science* **2014**, *345*, 542.
[22] M. Stolterfoht, C. M. Wolff, J. A. Márquez, S. Zhang, C. J. Hages, D. Rothhardt, S. Albrecht, P. L. Burn, P. Meredith, T. Unold, D. Neher, *Nat. Energy* **2018**, *3*, 847.
[23] Y. Lin, L. Shen, J. Dai, Y. Deng, Y. Wu, Y. Bai, X. Zheng, J. Wang, Y. Fang, H. Wei, W. Ma, X. C. Zeng, X. Zhan, J. Huang, *Adv. Mater.* **2017**, *29*, 1604545.
[24] F. Li, J. Yuan, X. Ling, Y. Zhang, Y. Yang, S. H. Cheung, C. H. Y. Ho, X. Gao, W. Ma, *Adv. Funct. Mater.* **2018**, *28*, 1706377.
[25] Q. Wang, Q. Dong, T. Li, A. Gruverman, J. Huang, *Adv. Mater.* **2016**, *28*, 6734.
[26] S. You, H. Wang, S. Bi, J. Zhou, L. Qin, X. Qiu, Z. Zhao, Y. Xu, Y. Zhang, X. Shi, H. Zhou, Z. Tang, *Adv. Mater.* **2018**, *30*, 1706924.
[27] J.-Y. Seo, R. Uchida, H.-S. Kim, Y. Saygili, J. Luo, C. Moore, J. Kerrod, A. Wagstaff, M. Eklund, R. McIntyre, N. Pellet, S. M. Zakeeruddin, A. Hagfeldt, M. Grätzel, *Adv. Funct. Mater.* **2018**, *28*, 1705763.
[28] L. Zuo, Q. Chen, N. De Marco, Y. T. Hsieh, H. Chen, P. Sun, S. Y. Chang, H. Zhao, S. Dong, Y. Yang, *Nano Lett.* **2017**, *17*, 269.
[29] H. Sun, K. Deng, Y. Zhu, M. Liao, J. Xiong, Y. Li, L. Li, *Adv. Mater.* **2018**, *30*, 1801935.
[30] J. Cao, B. Wu, R. Chen, Y. Wu, Y. Hui, B.-W. Mao, N. Zheng, *Adv. Mater.* **2018**, *30*, 1705596.
[31] A. Abrusci, S. D. Stranks, P. Docampo, H. L. Yip, A. K. Jen, H. J. Snaith, *Nano Lett.* **2013**, *13*, 3124.
[32] Y. Hou, X. Du, S. Scheiner, D. P. McMeekin, Z. Wang, N. Li, M. S. Killian, H. Chen, M. Richter, I. Levchuk, N. Schrenker, E. Spiecker, T. Stubhan, N. A. Luechinger, A. Hirsch, P. Schmuki, H.-P. Steinrück, R. H. Fink, M. Halik, H. J. Snaith, C. J. Brabec, *Science* **2017**, *358*, 1192.
[33] J. Peng, J. I. Khan, W. Liu, E. Ugur, T. Duong, Y. Wu, H. Shen, K. Wang, H. Dang, E. Aydin, X. Yang, Y. Wan, K. J. Weber, K. R. Catchpole, F. Laquai, S. De Wolf, T. P. White, *Adv. Energy Mater.* **2018**, *8*, 1801208.
[34] M. Kim, S. G. Motti, R. Sorrentino, A. Petrozza, *Energy Environ. Sci.* **2018**, *11*, 2609.
[35] F. Zhang, J. Song, R. Hu, Y. Xiang, J. He, Y. Hao, J. Lian, B. Zhang, P. Zeng, J. Qu, *Small* **2018**, *14*, 1704007.
[36] A. Kanevce, W. K. Metzger, *J. Appl. Phys.* **2009**, *105*, 094507.
[37] J.-T. Lin, S. Member, IEEE, C.-C. Lai, C.-T. Lee, Y.-Y. Hu, K.-Y. Ho, S. Haga, *IEEE J. Photovoltaics* **2018**, *8*, 669.
[38] P.-L. Qin, G. Yang, Z.-W. Ren, S. H. Cheung, S. K. So, L. Chen, J. Hao, J. Hou, G. Li, *Adv. Mater.* **2018**, *30*, 1706126.
[39] Y. Wu, P. Wang, S. Wang, Z. Wang, B. Cai, X. Zheng, Y. Chen, N. Yuan, J. Ding, W.-H. Zhang, *ChemSusChem* **2018**, *11*, 837.
[40] H. Bin, Z. G. Zhang, L. Gao, S. Chen, L. Zhong, L. Xue, C. Yang, Y. Li, *J. Am. Chem. Soc.* **2016**, *138*, 4657.
[41] Y. Zhao, H. Tan, H. Yuan, Z. Yang, J. Z. Fan, J. Kim, O. Voznyy, X. Gong, L. N. Quan, C. S. Tan, J. Hofkens, D. Yu, Q. Zhao, E. H. Sargent, *Nat. Commun.* **2018**, *9*, 1607.
[42] O. Malinkiewicz, A. Yella, Y. H. Lee, G. M. Espallargas, M. Graetzel, M. K. Nazeeruddin, H. J. Bolink, *Nat. Photonics* **2014**, *8*, 128.
[43] T. S. Sherkar, C. Momblona, L. Gil-Escrig, H. J. Bolink, L. J. A. Koster, *Adv. Energy Mater.* **2017**, *7*, 1602432.

